JAAS
Journal of Analytical Atomic Spectrometry

www.rsc.org/jaas

Volume 27 | Number 5 | May 2012 | Pages 709–898

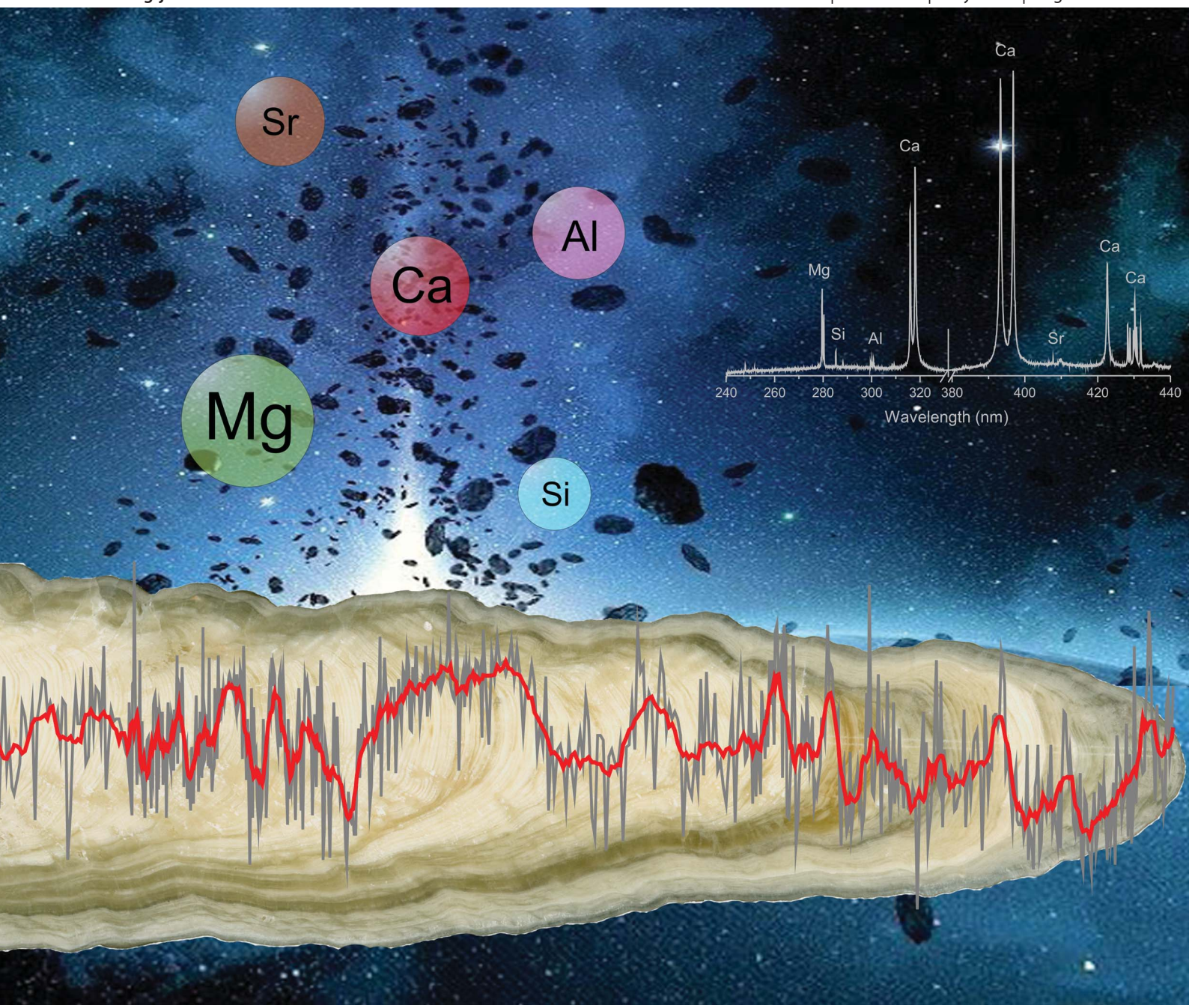

ISSN 0267-9477

RSC Publishing

PAPER
Laserna *et al.*
Spatial distribution of paleoclimatic proxies in stalagmite slabs using laser-induced breakdown spectroscopy

JAAS

Dynamic Article Links

Cite this: *J. Anal. At. Spectrom.*, 2012, **27**, 868

www.rsc.org/jaas

PAPER

Spatial distribution of paleoclimatic proxies in stalagmite slabs using laser-induced breakdown spectroscopy

F. J. Fortes,[a] I. Vadillo,[b] H. Stoll,[c] M. Jiménez-Sánchez,[c] A. Moreno[d] and J. J. Laserna*[a]

Received 6th October 2011, Accepted 2nd February 2012
DOI: 10.1039/c2ja10299d

The spatial distribution of paleoclimatic proxies in stalagmite slabs using laser-induced breakdown spectroscopy (LIBS) has been performed in this study. Stalagmites from different locations in the north of Spain were cut and analyzed along the main growth axis by LIBS. For comparative purposes, powders drilled from along the growth axis were also analyzed by inductively coupled plasma-atomic emission spectroscopy (ICP-AES). Advantages of LIBS include fast analysis of long stalagmite sections at atmospheric pressure, lateral resolution in the μm range and no sample preparation beyond having optical access to the stalagmite section to be inspected. Mg/Ca and Sr/Ca intensity ratios are of major interest for paleoclimate applications. An excellent agreement between the Mg/Ca intensity ratios measured in LIBS and in ICP-AES was observed. Sr/Ca trends were well matched only in high Sr stalagmites. Also, this work reports the employment of detrital layers as paleoclimatic proxies in speleothems by LIBS. Large concentrations of Si and Al are indicative of flood events inside the cave.

1. Introduction

A speleothem is a secondary mineral deposit formed in caves. These deposits have recently emerged as prime archives for paleoclimate studies. A close relationship between the hydrological conditions during speleothem formation and its growth rates and composition[1] has been demonstrated. Stalagmites (mostly comprised of $CaCO_3$ either as calcite or aragonite) are particularly useful for palaeoclimate applications, thanks to their relatively simple geometry. Elemental chemical indicators include the substitution rate of divalent cations (Sr, Mg, Ba) for Ca in its structure. In addition, elements associated with the detrital layer (aluminosilicate minerals; Al and Si) may be also trapped in stalagmites.[2–4] All of these parameters may be influenced by climatic processes. In this sense, Mg/Ca, Ba/Ca, and Sr/Ca concentration ratios are often monitored with the objective to correlate the speleothem composition with the climatic processes. In some cases, seasonal differences in climate or cave environments result in subannual scale geochemical variation in stalagmites. At typical stalagmite growth rates, annual layers may range from tens of microns to millimetres depending on the drip rate. Thus, the analysis of trace elements in speleothems at high spatial resolution is therefore desirable.

In the last few years, trace element concentration in stalagmites has been measured using a variety of analytical techniques including AAS, ICP-AES, ICP-MS, XAFS and SIMS, among others.[5,6] Wet chemistry techniques involve the extraction of discrete samples from the rock for dissolution and analysis. Alternatively, techniques that directly analyze the solid normally require the cutting of a small portion of the stalagmite for its inspection in a sample chamber, often of reduced size. Typically, less than 5 cm × 2 cm sections are required. In most cases the stalagmites of interest are much larger than the sample chamber. Thus, when information on the spatial distribution of an element across the rock is required the sample must be destroyed to a large extent. Laser-induced breakdown spectrometry (LIBS)[7–10] offers several advantages for the analysis of speleothems: fast analysis at atmospheric pressure, lateral resolution in the μm range, negligible sample preparation, good sensitivity and the capability of analysis without cutting the stalagmite into small portions.[11–13]

In a previous work, Vadillo *et al.*[14] applied LIBS for the spatially resolved analysis of major elements in speleothems taken from the *Nerja Cave* (Malaga). Because of the significance of these elements as paleoclimatic proxies, Mg and Sr were measured along the growth axis of the sample. In addition, the ablation process was studied taking into account several factors such as the presence of alteration layers and the roughness of the sample. In this study, LIBS revealed different patterns in the axial and growing directions for Mg and Sr. Authors suggest that this fact could be in agreement with geological data since dolomite includes higher levels of Mg while aragonite includes preferably Sr in its structure. Recently, a portable laser-induced plasma spectrometer was designed by Cuñat and co-workers[15]

[a]*Department of Analytical Chemistry, Faculty of Sciences, University of Malaga, Campus de Teatinos s/n, 29071 Malaga, Spain. E-mail: laserna@uma.es*
[b]*Department of Geology, Faculty of Sciences, University of Malaga, Campus de Teatinos s/n, 29071 Malaga, Spain*
[c]*Department of Geology, University of Oviedo, Oviedo, Spain*
[d]*Instituto Pirenaico de Ecología-CSIC, 50080 Zaragoza, Spain*

for the determination of thickness and composition of alteration layers on the surface of speleothems. The authors also evaluated the instrument inside the *Nerja Cave*. LIBS analysis revealed the presence of Fe, Si, Al and Mn in the alteration layer, which were absent in the bedrock. Different locations inside the cave were analyzed using the portable instrument. The Mg/Ca and Sr/Ca intensity ratios have been also studied by LIBS in hypercalcified sponges.[16] Most recently, multielemental analysis of a section of a stalagmite (6×12 mm^2) using LIBS has been reported.[17] The authors evaluated matrix effects by measuring the electron density and the electron temperature of the plasmas at different positions of the analyzed stalagmite, resulting in a negligible effect under their conditions. 2-D concentration maps of the trace elements were generated. In a recent study, Galbács *et al.*[18] applied a novel signal correction scheme based on the total integrated spectral background for the qualitative study of major and minor elements in stalagmite samples from Baradla Cave (Hungary). At a first instance, this approach allows one to solve the problems of signal fluctuations due to shot-to-shot instability, heterogeneity of the sample or even the defocusing effect caused if the sample surface moves out of focus during lateral translation. Although this signal correction has been successfully tested in these samples, several improvements are required for future applications.

The present work reports the spatial distribution of paleoclimatic proxies in stalagmite slabs using LIBS. Although the capability of LIBS for both laboratory and field applications has been demonstrated, the relationship between the LIBS paleoclimatic proxies and the age of the speleothem has not been reported before. In this paper, we reveal for the first time that LIBS is a useful tool to demonstrate the correlation between the chemical analysis and the age of the rock. Also, LIBS analysis has been compared with that obtained by ICP-AES and in both cases the Mg/Ca and Sr/Ca trends (measured along the growth axis of the samples) were in good agreement. Inclusion of detrital layers (Si and Al) in the speleothems is related to flood events occurring during the precipitation of $CaCO_3$. Although Si and Al could appear from a soil source, large concentrations of these elements are indicative of flood events inside the cave. In this sense, the intensity and event's frequency for Si and Al could establish models or patterns for wet periods in such areas. In addition, the use of detrital layers as paleoclimatic proxies in speleothems by LIBS has not been exploited before. Particularly interesting is the LIBS analysis of Si, a difficult element to analyze by ICP-AES because of its well-known insolubility in most acids. It should be noted that in this work we have not attempted a quantitative analysis by LIBS. The concentrations were indirectly obtained by ICP-AES. The main aim is to characterize models or patterns in the paleoclimatic proxies which allow us to correlate LIBS with other techniques ($\delta^{18}O$, $\delta^{13}C$, fluorescence of humic/fulvic laminations, lamination thickness, …). Thus, quantification is not considered relevant at this level.

2. Experimental set-up

2.1. Instrumentation

The overall system consists of a hand-held probe, a main unit and the laser power supply. Each of these parts is interconnected by means of an umbilical cable housing the fiber optic cable, trigger signal cable, I/O and refrigeration lines among others. These blocks can be easily split, permitting effortless transportation of the instrument separately. The main unit has an overall weight of approximately 5 kg and a size of $45 \times 27 \times 15$ cm^3. Moreover, the main unit is a specially adapted backpack where both the spectrometer and the personal computer are enclosed. Conversely, the laser head and all the optical arrangements are housed in the hand-held probe. A fibre optic cable guides the plasma emission from the probe to the spectrograph. The entire system is controlled wirelessly by means of a hand-held PDA device that permits data visualization as well as control of the spectrometer and the laser parameters. While this work was carried out in the lab, the system was designed for field analysis.

The plasma was generated using a Q-switched Nd:YAG laser, operating at its fundamental wavelength and generating a laser pulse energy of 50 mJ of 6.5 ns in length. The laser beam was focused onto the target surface by a BK7 75.6 mm focal-length lens with a 1064 nm antireflexive coating. Then, the plasma emission was directly collected by a fiber optic cable (5 m length, 600 μm diameter, 0.22 NA) and guided to the 10 μm slit of a compact spectrometer located at the main unit of the instrument. The spectrometer (Ocean Optics HR2000) consists of a 1/10 m crossed Czerny–Turner scheme with a holographic diffraction grating of 2400 lines mm^{-1} and a CCD array dotted with 2048 elements where the dispersed light is finally detected. This configuration provides time-integrated LIBS spectra with 0.05 nm pixel^{-1} resolution. In this way, two spectrometers could be employed covering the 240–460 nm spectral range. The SMA connector and plug and play configuration of the spectrometer permit easy swapping of the spectrometers. The system also incorporated a built-in compact PC board that controlled the above-mentioned components as well as the acquisition and processing routines. A LabView® program was developed to control both the laser and the spectrometer and to perform data processing. The program was designed to allow real-time spectra acquisition and depth profile visualization of any particular spectral line.

2.2. Samples

A set of 6 speleothems from Asturias (north of the Iberian Peninsula) have been analyzed by LIBS and ICP-AES. The samples represent a range of growth rates and several different cave settings with different karst bedrock formations, providing a range of textures, ages, and absolute chemistry of the speleothems. Additional information regarding the samples analyzed in this work is summarized in Table 1. The samples were cut along

Table 1 Description and additional information concerning the stalagmites analyzed by LIBS and ICP-AES

Sample	Length/mm	Location
PIN	290	Pindal Cave
MAR	470	Pindal Cave
CAN	420	Pindal Cave
ANG	860	Las Bolugas Cave
KRI	85	Fría Cave
ADAM	145	Fría Cave

the growing axis without any chemical preparation. LIBS and ICP analyses were completed in two complementary halves of the cut speleothem, allowing comparison of the overall trends but not variations at the mm scale.

Trace element chemistry and detailed age models for the *CAN* sample are reported elsewhere by Moreno *et al.*[19] For *MAR, ANG* and *PIN* samples we show an approximate estimate of the duration of the record by plotting the chemical evolution on a time scale based on a few initial age determinations by U/Th using techniques described elsewhere.[19]

2.3. Sample preparation

For the ICP-AES analysis, stalagmites were analyzed using matrix-matched standards on a simultaneous dual ICP-AES (Thermo ICAP DUO 6300). Samples were drilled every 1 mm (the spot size in ICP drilling is double that of LIBS ablation) and represent averages of decadal to centennial intervals integrating over any seasonal cycle in trace element concentrations. Then, drilled powder was placed in tubes previously cleaned with 10% HCl and triply rinsed in Milli-Q water. Samples were dissolved in 1.5 mL of 2% HNO_3 (Tracepur) immediately prior to analysis and were introduced with a microflow nebulizer (0.2 mL min^{-1}) which permitted two replicate analyses. The use of small sample volumes allowed high sample concentrations and detection of a range of trace elements present at low abundances. Calibration was conducted off-line using the intensity ratio method described by de Villiers *et al.*[20]

The spot size in LIBS analysis was measured to be 450 μm. Data were obtained by averaging 20 laser shots at each sample position after 5 laser shots used for cleaning purposes while the lateral resolution was established at 500 μm. On the other hand, the paleoclimatic years represented by the spot size depend on the speleothem growth rate (due to the drip rate inside the cave) in each particular case.

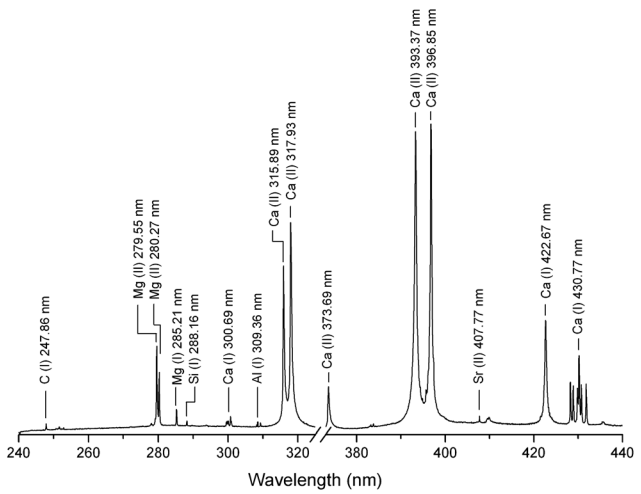

Fig. 1 LIBS spectra corresponding to the matrix of a speleothem in the spectral window covering the range 240–440 nm. Emission lines of Al, C, Ca, Mg, Si and Sr are labelled in the spectra.

3. Results and discussion

The LIBS spectrum of the *PIN* sample in the spectral window covering the range from 240 nm to 440 nm is presented in Fig. 1. In addition to Ca and Mg, emission lines of Al, C, Si and Sr were also identified. Average intensities for these elements on *CAN, MAR, ANG* and *PIN* samples are summarized in Table 2. Although the LIBS analysis was made along the growing axis, which means the bedrock of the sample, an external alteration layer was also well identifiable.[15] It should be noted that the lateral displacement of the sample surface during the scanning could affect the signal intensity if the sample moves out of the focus.[18] In our experiment, this defocusing effect has been solved since samples were positioned in a high-precision *x–y–z* motorized stage ensuring that the laser beam was normal to the sample surface along the full scan path.

According to the results presented in Table 2, variations in the LIBS signal appear to vary significantly along the speleothem growth axis in all samples. The intensity of Ca varies more than 5-fold with relative standard deviations in the range of 15–25% although $CaCO_3$ is always the dominant component (>97% in all stalagmites). On the other hand, the Ca signal appears to be highest in sections of the stalagmite which exhibit larger porosity. It is well known that roughness and heterogeneity on the sample surface have an effect on the laser–matter interaction during laser ablation. This fact induces changes in the ablated mass and consequently in the intensity of all species in the plume. Variations in the LIBS signal affect not only the Ca intensity but also Mg, Sr, Si and Al intensities. This fact makes the use of ratios of elements more reliable than simple intensity measurements. Taking into account that stalagmites are mainly $CaCO_3$, the use of Ca as an internal standard is totally justified in this work. Additionally, the ratio of the intensity of other elements (Sr, Mg) to Ca intensity refers to the substitution rate of divalent cations for Ca in the structure of $CaCO_3$. From these considerations, in this manuscript we report the variations in intensity ratios of minor and trace elements to calcium. The emission lines of

Table 2 Average LIBS intensity and standard relative deviation of Mg, Si, Al, Sr and Ca for the samples analyzed along their growing axis

	Mg		Si		Al		Sr		Ca	
Sample	AVG intensity	RSD (%)	AVG intensity	RSD (%)	AVG intensity	RSD (%)	AVG intensity	RSD (%)	AVG intensity	RSD (%)
PIN	9770	31.8	1839	34.6	1346	28.8	1722	20.0	17 526	23.9
MAR	6042	28.6	1112	14.0	1137	15.2	1415	16.9	15 652	15.4
CAN	5738	32.1	1118	21.5	1319	22.6	1375	30.6	15 550	18.7
ANG	4707	47.5	991	41.0	947	38.0	950	25.0	13 092	25.5
KRI	4524	28.3	1827	27.0	1610	27.1	—	—	22 702	24.9
ADAM	3602	25.6	1518	22.8	1341	24.4	—	—	19 389	19.2

C(I) 247.86 nm, Mg(I) 285.21 nm, Si(I) 288.16 nm, Al(I) 309.36 nm, Ca(II) 317.93 nm and Sr(II) 407.77 nm were used in this study. These lines were selected in order to avoid self-absorption, saturation or even the overlapping with other emission lines. Nevertheless, the same results were obtained when using other lines different to that described here.

3.1. LIBS analysis of divalent cations in speleothem calcite

As observed in Table 2, among the minor/trace elements, Mg yielded the highest intensity in LIBS spectra and is inferred to be the most reliably measured trace element by this method. Moreover, Mg is typically present in speleothems at higher concentrations in comparison to other trace metals. In addition, the Mg/Ca intensity ratio has great interest as a paleoclimatic proxy.

The Mg/Ca variation in the different speleothems analyzed by LIBS and ICP-AES is shown in Fig. 2. The concentrations measured by ICP-AES are not normalized to the Ca concentration. The *x*-axis was converted from distance along the growing axis to timescale according to a radiometric dating method. From a paleoclimatic perspective, this conversion is of great importance since it allows the Mg/Ca variation to be related to the age of the speleothem. The red and blue curves that appear in the graphs are fitting lines over the gray points representing both LIBS and ICP analysis. As observed, Mg/Ca LIBS measurements in calcite reproduce well the Mg variations measured by ICP-AES. However, when analyzed in more detail there are differences in LIBS and ICP-AES trends in certain sections of some stalagmites which are most noticeable in the *PIN* sample (Fig. 2A). In this case, the unusually large Mg/Ca ratio observed in LIBS in the upper (most recent) portion of the stalagmite could be due to a strong change in porosity of the rock. As commented, the laser ablation phenomenon is altered by several parameters (roughness, porosity, color, heterogeneity and hardness, among others) which directly affects the optical emission. In fact, there is an increase in detrital content indicated by a reddish color in this section of the stalagmite. Moreover, detrital Mg may be represented more completely by the ablation used in LIBS than with the acid dissolution method used in ICP-AES. Small differences in some sections of the *MAR* sample are observed (Fig. 2B) although the general trend is equivalent in both methods. On the other hand, in *CAN* (Fig. 2C) and *ANG* (Fig. 2D) samples ICP and LIBS data correlate fairly well. These two stalagmites are characterized by very pure dense calcite. Consistency in texture, minimal porosity, and absence of detrital components are contributing factors to this agreement.

To confirm the accuracy of the LIBS measurements we compared LIBS and ICP-AES measurements for *ANG* and *CAN*. Fig. 3 compares the Mg/Ca intensity LIBS ratio as a function of Mg concentration (mmol mol^{-1}) measured by ICP-AES along the growing axis for these samples. The data show a strong positive correlation between the two series although the intercept of LIBS and ICP-AES appears to differ slightly between the two stalagmites studied. Nevertheless, the correlation coefficients calculated (0.89 and 0.96 for *ANG* and *CAN*, respectively) confirm a good correlation between both techniques. Overall, the most interesting capability of LIBS is in

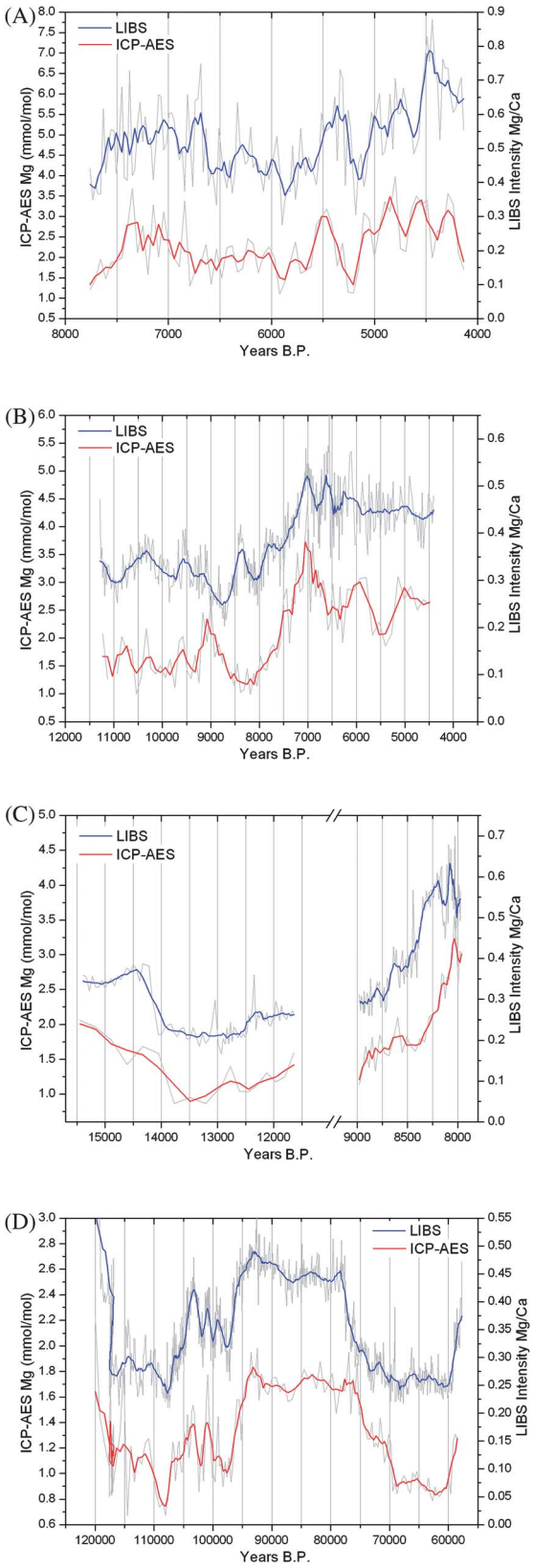

Fig. 2 LIBS lateral profile of the Mg/Ca intensity ratio along the growing axis for the different speleothems analyzed: (A) *PIN*, (B) *MAR*, (C) *CAN* and (D) *ANG*; age scale for A, B, and D is approximate based on initial U/Th age determinations. For the sake of comparison, Mg measured by ICP-AES is also plotted.

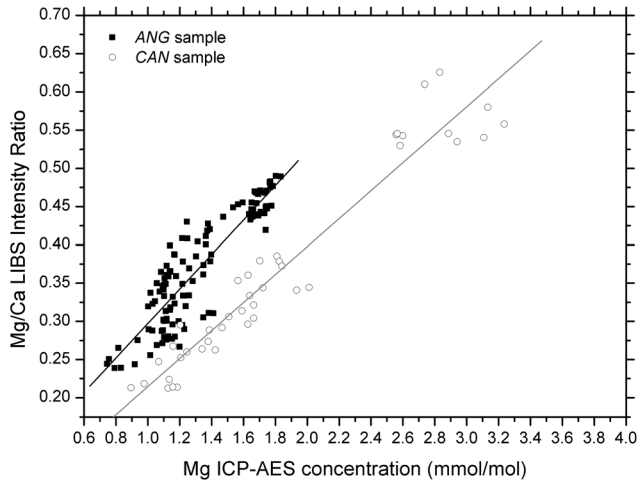

Fig. 3 Correlation of the results obtained with LIBS and ICP-AES for the *ANG* sample (■, black line) and *CAN* sample (○, light gray line).

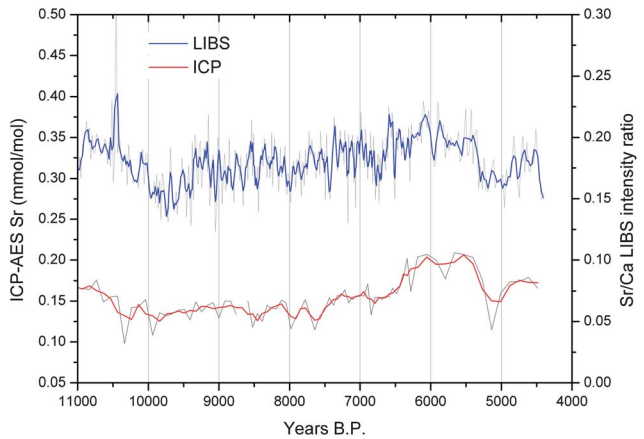

Fig. 4 LIBS lateral profile of the Sr/Ca intensity ratio along the growing axis for the *MAR* sample. For the sake of comparison, Sr measured by ICP-AES is also plotted.

Mg/Ca ratios where it can be a useful screening tool and permits high speed analysis of long speleothems.

On the other hand, the concentration of strontium in calcite and its importance in geochemistry as a paleoclimatic proxy[1,3,14] were also of interest in this study. However, the abundance of Sr in these speleothems appears to be close to the limit of the detection of LIBS and only those samples presenting an average Sr concentration higher than 0.2 mmol mol^{-1} show a strong correlation between the Sr/Ca intensity LIBS ratio and the Sr concentration measured *via* ICP-AES. As an example, Fig. 4 shows a representative LIBS lateral profile of the Sr/Ca intensity ratio along the growing axis for the *MAR* sample. For comparative purposes, the Sr concentration measured by ICP-AES is also plotted. In this case, the correlation between data obtained in both techniques matched well along the growing axis. From these data it is clear that Sr/Ca trends were well matched in samples having a large Sr concentration.

3.2. LIBS measurements of detrital compounds in speleothems

In certain caves the delivery of detrital minerals on growing stalagmites can be related to climate changes, either through climatically controlled condensation of speleothem growth (hiatus of $CaCO_3$ deposition) or through episodic deposition of detrital materials during flooding of caves. Detrital layers may be distinguished as enrichments in the concentration of Si and Al. The signal of these events is also recorded during the growing of the stalagmites. To check for the capability of LIBS for this application, LIBS Si/Ca and Al/Ca profiles along the growing axis of several stalagmites were studied. Fig. 5 shows the results for *KRI* and *ADAM* samples (which are twin stalagmites separated only by a few cm in their original location and slow growing with very slow drips). As shown, the Al/Ca profile reproduces exactly in both cases the behaviour of Si/Ca along the growing axis. This fact confirms that Si and Al are closely related to the detrital layer. The intervals of elevated Al/Ca and Si/Ca correspond with intervals of visible bands of tan coloring in the stalagmite, interpreted as greater detrital abundance. Detrital enriched layers are believed to represent flood events and the

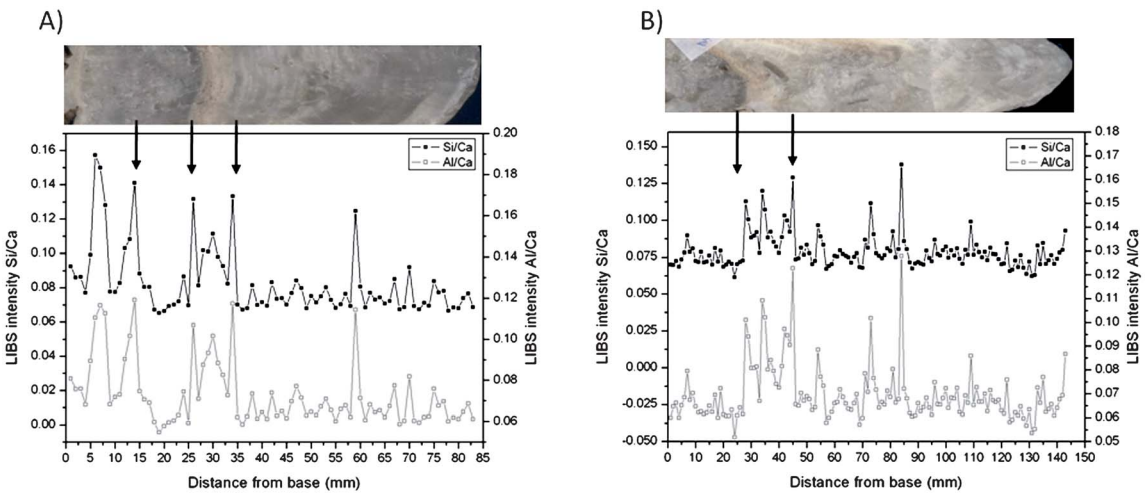

Fig. 5 Si/Ca and Al/Ca intensity ratios measured by LIBS in samples (A) *KRI* and (B) *ADAM*. The abscissa axis represents the distance along the growing axis of the speleothem. Black arrows indicate the presence of inclusions of detrital layers in both speleothems.

amount of detrital minerals proportional to flood intensity or frequency. LIBS offers a very interesting alternative for such studies, since Si and Al are only weakly soluble in acids as required in ICP-AES and AAS.

4. Conclusions

In this work LIBS has been successfully applied for the spatial distribution of paleoclimatic proxies in stalagmite slabs belonging to different karstic caves in the Iberian Peninsula. LIBS has been demonstrated to be a useful screening tool allowing high speed analysis of large speleothems. Due to their importance as paleoclimatological and paleohydrological indicators, Mg/Ca variations were analyzed along the growing axis of the stalagmite. An excellent agreement between the Mg/Ca intensity ratios measured by LIBS and by ICP-AES was observed. The correlation coefficients calculated (0.89 and 0.96 for *ANG* and *CAN*, respectively) when comparing ICP-AES and LIBS data confirm a good correlation between both techniques. On the other hand, Sr/Ca variation in LIBS and ICP-AES analysis was only well matched in those stalagmites presenting a high Sr content.

In addition, the employment of detrital layers (Si and Al) as paleoclimatic proxies in speleothems by LIBS has been performed in this report. Although Si and Al could appear from a soil source, large concentrations of these elements are indicative of flood events inside the cave. Moreover, the Al/Ca profile reproduces exactly the behaviour of Si/Ca along the growing axis. This fact confirms that Si and Al are closely related to the detrital layer which may indicate flood events in the karstic cave. In this sense, the intensity and event's frequency for Si and Al could establish models or patterns for wet periods in such areas.

Acknowledgements

Research was supported by project CTQ 2007-60348 of the Spanish Ministerio de Ciencia e Innovación. It is also a contribution to the Research Group RNM-308 (Group of Hydrogeology) of the Junta de Andalucía (Spain). This project was supported by a grant from the Spanish Ministry of Education and Science (CAVECAL: MEC CGL2006-13327-Co4-02) by an instrumentation grant to H. Stoll from the Asturian Commission of Science and Technology (FICYT 2006) co-financed by the European Regional Development Funds.

References

1 I. Fairchild and P. Treble, *Quat. Sci. Rev.*, 2009, **28**, 449–468.
2 A. Baker, D. Genty, W. Dreybrodt, W. L. Barnes, N. J. Mockler and J. Grapes, *Geochim. Cosmochim. Acta*, 1998, **62**, 393–404.
3 Y. M. Huang, I. J. Fairchild, A. Borsato, S. Frisia, N. J. Cassidy, F. McDermott and C. J. Hawkesworth, *Chem. Geol.*, 2001, **175**, 429–448.
4 J. U. L. Baldini, F. McDermott and I. J. Fairchild, *Science*, 2002, **296**, 2203–2206.
5 L. M. A. Purton-Hildebrand, G. W. Grime, G. A. Shields and M. D. Brasier, *Nucl. Instrum. Methods Phys. Res., Sect. B*, 2001, **181**, 506–510.
6 S. Frisia, A. Borsato, I. J. Fairchild and J. Susini, *Earth Planet. Sci. Lett.*, 2005, **235**, 729–740.
7 A. W. Miziolek, V. Palleschi and I. Schechter, *Laser Induced Breakdown Spectroscopy (LIBS) Fundamentals and Applications*, Cambridge University Press, Cambridge, UK, 2006.
8 D. A. Rusak, B. C. Castle, B. W. Smith and J. D. Winefordner, *Crit. Rev. Anal. Chem.*, 1997, **27**, 257–290.
9 J. D. Winefordner, I. B. Gornushkin, D. Pappas, O. I. Matveev and B. W. Smith, *J. Anal. At. Spectrom.*, 2000, **15**, 1161–1189.
10 I. Scaffidi, S. M. Angel and D. A. Cremers, *Anal. Chem.*, 2006, **78**, 25–32.
11 C. López-Moreno, S. Palanco, J. J. Laserna, F. DeLucia, Jr, A. W. Miziolek, J. Rose, R. A. Walters and A. I. Whitehouse, *J. Anal. At. Spectrom.*, 2006, **21**, 55–60.
12 F. J. Fortes, M. Cortés, M. D. Simón, L. M. Cabalín and J. J. Laserna, *Anal. Chim. Acta*, 2005, **554**, 136–143.
13 F. J. Fortes, J. Cuñat, L. M. Cabalín and J. J. Laserna, *Appl. Spectrosc.*, 2007, **61**, 558–564.
14 J. M. Vadillo, I. Vadillo, F. Carrasco and J. J. Laserna, *Fresenius' J. Anal. Chem.*, 1998, **361**, 119–123.
15 J. Cuñat, S. Palanco, F. Carrasco, M. D. Simón and J. J. Laserna, *J. Anal. At. Spectrom.*, 2005, **20**, 295–300.
16 C. Fabre and B. Lathuiliere, *Spectrochim. Acta, Part B*, 2007, **62**, 1537–1545.
17 Q. L. Ma, V. Motto-Ros, W. Q. Lei, M. Boueri, L. J. Zheng, H. P. Zeng, M. Bar-Matthews, A. Ayalon, G. Panczer and J. Yu, *Spectrochim. Acta, Part B*, 2010, **65**, 707–714.
18 G. Galbács, I. Kevei-Bárány, E. Szőke, N. Jedlinszki, I. B. Gornushkin and M. Z. Galbács, *Microchem. J.*, 2011, **99**, 406–414.
19 A. Moreno, H. Stoll, M. Jiménez-Sanchez, I. Cacho, B. Valero-Garcés, E. Ito and R. L. Edwards, *Global Planet. Change*, 2010, **71**, 218–231.
20 S. de Villiers, M. Greaves and H. Elderfield, *Geochem., Geophys., Geosyst.*, 2002, **3**, 1001–1014.